Performance Improvement of Concentrated-Flux Type IPM PMSM Motor with Flared-Shape Magnet Arrangement

Keun-Young Yoon [1] and Soo-Whang Baek [2],*

[1] Department of Electric Engineering, Honam University, 417 Eodeung-daero, Gwangsan-gu, Gwangju 62399, Korea; ky.yoon@honam.ac.kr

[2] Department of Human Intelligence and Robot Engineering, Sangmyung University, Cheonan 31066, Korea

* Correspondence: swbaek@smu.ac.kr; Tel.: +82-041-550-5548

check for updates

Featured Application: We propose a new replaceable rotor shape of an interior permanent magnet (IPM) motor to be used in electric water pump (EWP) systems of electric vehicles. The proposed structure can reduce the torque ripple and improve efficiency characteristics of the basic IPM permanent magnet synchronous motor (PMSM).

Abstract: This study demonstrates that the use of a flared-shape rotor structure in interior permanent magnet (IPM) permanent magnet synchronous motor (PMSM) yields better performance than the basic IPM PMSM motor, using a spoke structure with ferrite magnets. To concentrate the effective magnetic flux, the proposed rotor structure is composed of a number of ferrite magnets, which are inserted in a flared shape in the rotor core. This paper shows the comparison with the analysis results of 2D finite element method (FEM), and it is shown that the proposed IPM PMSM motor can be an effective substitute for the basic IPM PMSM motor, which requires low torque ripple and high efficiency. In particular, the proposed flared IPM PMSM motor has lower pulsation of torque and superior efficiency, as well as lower acoustic noise and vibration, compared to the basic IPM PMSM motor. To verify the performance improvement of the proposed model, a prototype of the proposed model was manufactured. It was experimentally confirmed that the proposed model has lower torque ripple and higher efficiency than the basic model. Based on this performance improvement, the proposed flared IPM PMSM motor is suitable for electric vehicles and home appliances.

Keywords: electric vehicles; electric water pump system; permanent magnet synchronous motor; interior permanent motor; spoke rotor structure; flared-shape rotor structure; ferrite magnet

1. Introduction

The permanent magnet synchronous motor (PMSM) is widely used in the electric vehicle and domestic appliance industries. The structure of the PMSM motor varies depending on the permanent magnet arrangement in the rotor structure; among them, the interior permanent magnet (IPM) PMSM motors made by inserting permanent magnets into rotors have advantages in applications requiring high output power and high efficiency at load condition [1–4]. In particular, IPM type motors have saliency depending on rotor shape. Because of, reluctance torque components can be obtained in addition to magnetic torque components. Thus, the total torque of IPM PMSM motors is higher than that of surface permanent magnet (SPM) PMSM motors, which comprise only magnet torque [5–9].

Several advanced studies have been conducted to improve motor properties through proposed novel structure and topology for the motor, considering the advantages of this IPM type motor.

In Reference [10], in order to increase the efficiency of the motor and achieve a wide operating range at the same time, an optimal design for a concentrated flux type interior permanent magnet (CFIPM) motor with a concentrated flux was proposed. In References [11,12], a concentrated flux type ferrite magnet motor using a ferrite magnet was proposed to improve the efficiency of the motor. Since the concentrated flux type permanent magnet motor has a high torque density, there are various attempts to replace the performance of rare earth magnet motor with the concentrated flux type motor using ferrite magnet. In References [13,14], a new structure was proposed for the concentrated flux type synchronous motor (CFSM) to improve torque density and vibration characteristics. To increase torque density, structures for improved motors were proposed using three different types of rotor core structures. In References [15–18], studies were conducted to reduce torque ripple. When the cogging torque characteristic of the motor is large, accuracy of position and speed control is reduced, which can increase the torque ripple. Therefore, the effect of the main design parameters of the motor for the reduction of cogging torque were accurately predicted and analyzed. In Reference [19], a design method was explored to adopt the same topology with two rotors, with one inner coreless stator, to improve the mechanical and electromagnetic performance of the motor. In Reference [20], the magnetic field calculation and performance characteristics of a transverse flux machine (TFM) with permanent magnet excitation were studied. The composition, magnetic flux distribution, the back electro-motive force (EMF) and winding inductance characteristics of the TFM were analyzed, and the effectiveness of a simplified computational model was verified. In Reference [21], a type of transverse flux reluctance machine was studied. However, this design had the drawback of having a high fundamental frequency and high torque ripple, which complicate the control of the motor. To address this, a magnetic material study was conducted that could use a complex magnetic stator shape with a 3D magnetic flux path using a soft magnetic composite (SMC) in the magnetic circuit.

In this study, we will compare the characteristics of the basic IPM model (the spoke structure) and the proposed flared type IPM model (the flared structure). In our previous study, two types of concentrated flux type IPM motors with the flared-shape magnets arrangement were examined. The flared type IPM model adopts a flared structure of C-shape ferrite magnets [22]. The proposed flared-shape structure can increase the useful magnetic flux, so the flared type IPM motor is also a form of the concentrated flux type IPM motor. The proposed flared-shape structure is optimized, and the validity is verified experimentally [23]. The study proposes a flared type rotor structure for replacing the basic spoke type IPM model, for performance enhancement. Additionally, the study aims to determine possible alternatives and performance improvements through performance comparisons. In particular, since the proposed model has advantages such as low torque ripple and reduction of electromagnetic force causing noise vibration, it is necessary to apply the model in electric vehicles and home appliances. In this study, the proposed model replaces the basic model used in the electric water pump (EWP) system of electric vehicles. First, finite element method (FEM) analysis is used to compare performance and determine whether it has improved. Subsequently, we compare the results of the prototype analysis with those of the experiments. Finally, the improved performance and replacement suitability of the proposed model were experimentally verified.

2. Structures of Basic Spoke Type IPM Model and Proposed Flared Type IPM Model

2.1. Electric Water Pump System

The engine cooling system maintains the temperature in the engine room at the required level. If the temperature in the engine room is extremely high during vehicle operation, the component strength of the engine cooling system decreases. Therefore, the engine cooling system is an important device that keeps the temperature in the engine room at the desired level. The traditional engine cooling method of a vehicle is a mechanical driving cooling technique that rotates a water pump pulley using the driving force transmitted through a crankshaft. Recently, the electric and hybrid automobile

market that requires high power and high responsiveness is expanding. In particular, the electric water pump market driven by electric motors is also expanding.

An electric water pump system consists of three parts: cooling water that lowers the temperature of the engine room, IPM motor that is responsible for the rotation of cooling water, and the controller. IPM motors must satisfy high efficiency requirements because they use energy supplied from the inside of the vehicle. In addition, since the engine cooling system is installed close to the engine room, the torque ripple or excitation source of the IPM motor can cause noise vibration. Therefore, various attempts have been made to improve the performance of EWP motors and to reduce torque ripple.

Figure 1 shows a 300 W EWP motor and the motor shape mounted inside. The IPM motor was applied as a driving source.
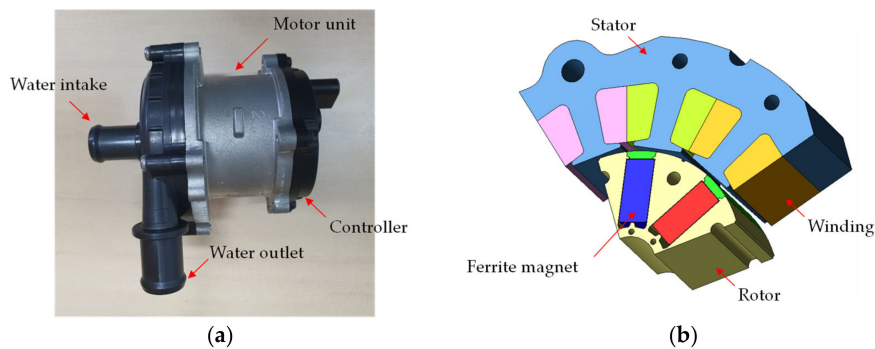

Figure 1. Electric water pump system: (**a**) configuration and major components; (**b**) basic motor unit.

2.2. Basic Spoke Type IPM Model

Figure 2 shows the shape of the basic spoke type IPM model in which a permanent magnet is magnetized in a concentrated flux structure (white mark). As shown in Figure 2, the basic spoke type IPM model is applied with 8 poles and concentrated winding. The multi-polar structure of the IPM model and the concentrated winding have a high output power density per unit volume and high efficiency, so this model has been widely used in fields such as home appliances and electric vehicles. Additionally, the spoke type motor is better at concentrating magnetic flux than other IPM motors. Therefore, the magnetic flux can be utilized more efficiently and the output power density can be increased. In order to prevent the problem of scattering during high-speed rotation, the rotor structure is designed with an interior permanent magnet and composed of plastic resin, which is effective even in high-speed rotation. Moreover, the basic spoke type IPM model uses ferrite magnets of grade 9BE, which cost less than NdFeB magnets. Therefore, this model has a price advantage, and can be applied to electric vehicles and household appliances. Table 1 shows the specification of the basic spoke type IPM model.
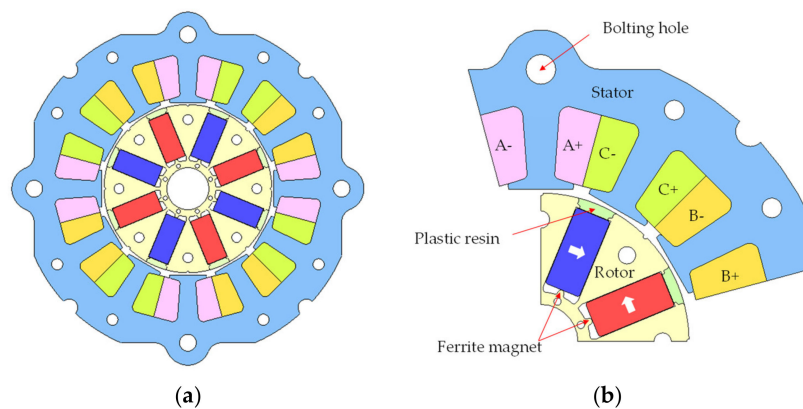

**Figure 2.** Structure of basic spoke type interior permanent magnet (IPM) model: (**a**) full model; (**b**) 1/4 model.

Table 1. Specifications of the basic model and proposed model.

	Item	Unit	Basic Model	Proposed Model
	Slot/Pole	-	12/8	12/8
	Output power	W	300	300
	Speed	rpm	4020	4020
Stator	Stack length	mm	27.5	27.5
	Outer diameter	mm	120.0	120.0
	Material	-	35PN270	35PN270
Rotor	Stack length	mm	27.5	27.5
	Outer diameter	mm	60	60
	Material	mm	35PN270	35PN270
	Air-gap	mm	0.75	0.75
Magnet	Shape	mm	Bar-type	C-type
	Dimensions	mm	$16.5 \times 7.4t$	$70deg \times 3.4t$
	Material	-	Ferrite (9BE)	Ferrite (9BE)
Winding	Number of turns	turns	30	30
	Diameter	mm	0.9	0.9
	Material	-	Copper	Copper

2.3. Characteristics of the Basic Spoke Type Ferrite IPM Model

The performance analysis of motors can be divided into two main categories. First, the no-load analysis confirms the winding specifications and the rotor geometry. Permanent magnet grade and winding specifications are checked through the magnitude of the back EMF; the shapes of the rotor and the stator are evaluated through the generated the back EMF waveform. Load analysis confirms torque magnitude and ripple at the rated speed, and efficiency at the rated load point is confirmed through copper and iron loss analysis. The noise vibration generation is compared relatively through torque ripple and nodal force analysis.

The characteristics of the basic spoke type IPM model were investigated by conducting no-load and load analyses on the basic spoke type IPM model. Figures 3 and 4 show the back EMF waveform and the cogging torque waveform from the no-load analysis. The back EMF is generated by a sinusoidal waveform, generating 23.65 Vrms per phase, and the THD (total harmonic distortion) of the back EMF is 0.69%.
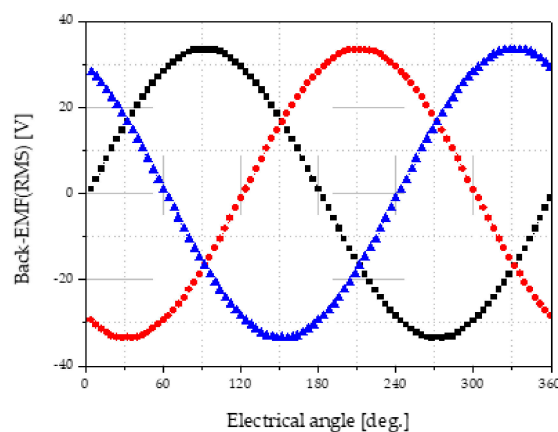
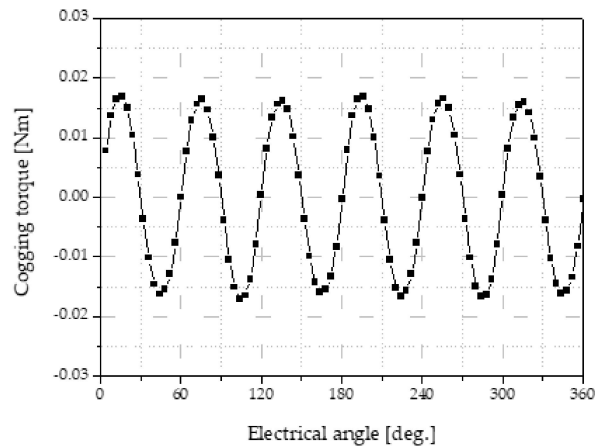**Figure 3.** Back EMF of basic spoke type IPM model.

Figure 4. Cogging torque of basic spoke type IPM model.

Table 2 shows the results of the performance analysis of the basic spoke type model under no-load and load conditions. The torque ripple at rated load is 0.068 Nm and the ripple rate is 9.4% based on the magnitude of the average torque. The efficiency is 92.7% at rate load.

Table 2. Characteristics of the basic spoke type ferrite IPM model.

	Item	Unit	Basic Model
No-Load	Back EMF	Vrms	23.65
	THD	%	0.69
	Cogging torque ripple	Nm	0.034
Load	Rated speed	rpm	4020
	Average torque	Nm	0.72
	Torque ripple (ripple rate)	Nm	0.068 (9.4%)
	Phase current	Apeak	6.0
	Output power	W	303.7
	Copper loss	W	14.4
	Iron loss	W	9.3
	Efficiency	%	92.7

In the case of a motor using a permanent magnet, the teeth of the stator are excited by the electromagnetic force of the permanent magnet inside the rotor, when the rotor rotates at a rated speed. Electromechanical force with the teeth of the stator eventually causes noise and vibration of the motor. The analysis of electromagnetic force must be performed in the load analysis, and nodal force analysis is mainly performed to calculate the electromagnetic force.

Figure 5 shows the nodal forces that are applied to the stator teeth of the basic spoke type IPM motor. When the rotor is rotated, the nodal force in the teeth region has two components. As shown in Figure 5, it has the x-axis components along the direction of rotation and y-axis components perpendicular to the direction of rotation. In particular, the y-axis component is perpendicular to the electromagnetic force, which is the main cause of noise vibration [24,25].
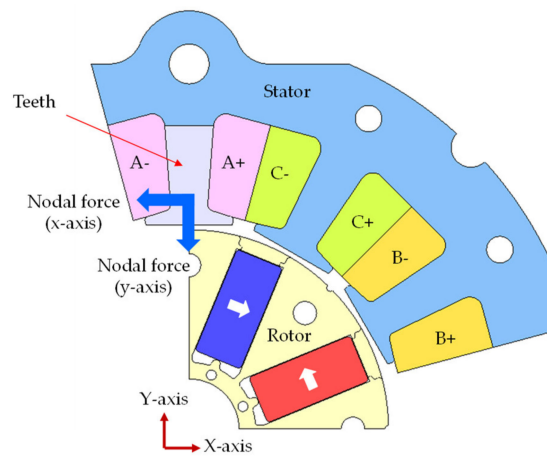
Figure 5. Nodal force components of the stator teeth.

Figure 6 shows a nodal force waveform applied to teeth under rated load conditions, and Table 3 shows a nodal force component along the x-axis and y-axis. As shown in Table 3, the y-axis directional component of the nodal force is greater than the x-axis component.
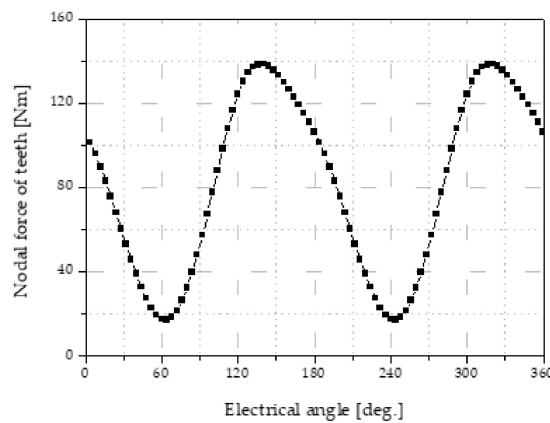

Figure 6. Nodal force of the stator teeth (absolute component).

Table 3. Nodal force component in x-axis and y-axis directions.

Item		Unit	Basic Model
Nodal force (peak to peak)	x-axis	Nm	10.93
	y-axis	Nm	121.24

2.4. Proposed Flared Ferrite IPM Model

In this paper, we propose a new model with a flat rotor shape to replace the existing model and improve performance. The flared-shape structure has several C-shaped ferrite magnets arranged in a flared shape in the rotor. The flared-shape structure of the ferrite magnets maximizes the utilization of the ferrite magnets in the rotor core. Thus, the flared type structure can concentrate the magnetic flux, which is caused by the arrangement of the magnets.

Figure 7 shows the structure of the proposed flared type IPM model, which has 12 slots /8 poles and concentrated winding, and a permanent magnet is magnetized in a concentrated flux structure (white mark). One pole consists of four C-shaped magnets, which are arranged in a flared shape. Figure 8 shows the design process of IPM motors. In this paper, the permanent magnet weight of the proposed model is set to be the same as that of the basic model, and then a flared magnet arrangement structure is designed for the rotor.
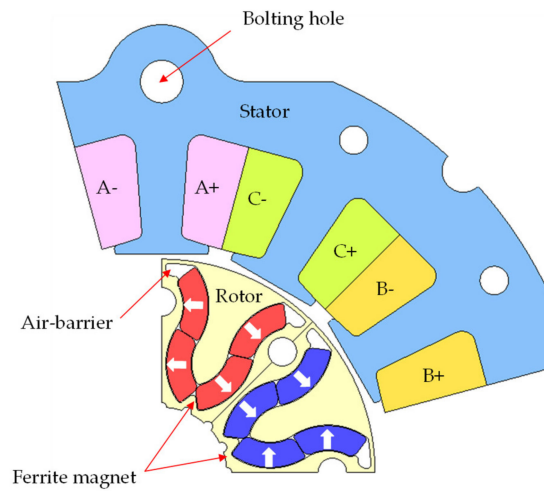
Figure 7. Structure of the proposed flared ferrite IPM model (1/4 model).
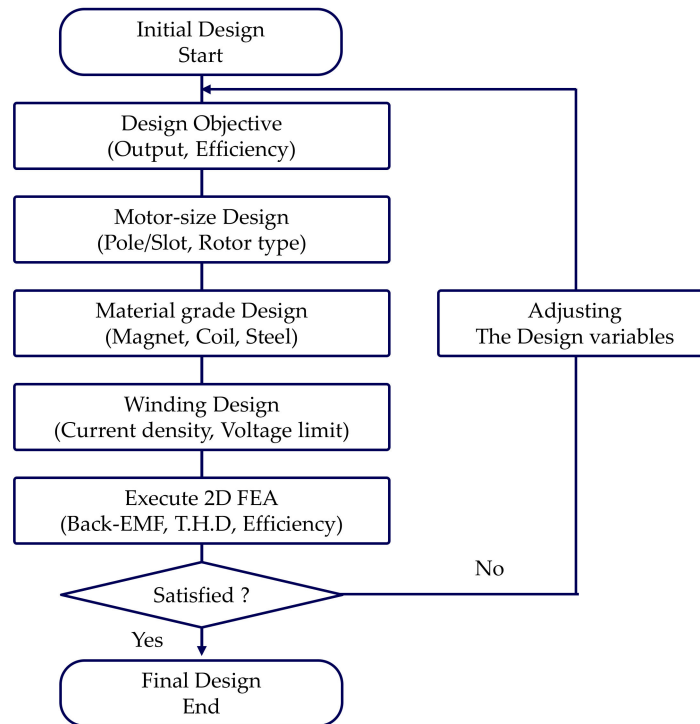

Figure 8. Design process of IPM motor.

Figure 9 shows the magnetization pattern of the proposed flared type IPM model. As shown in Figure 9a,b, the proposed flared type IPM model can have two different patterns (parallel and radial directions) and the magnetization pattern of the permanent magnet can determine the manufacturing process of the permanent magnet. The magnetic flux density distribution inside the rotor resulting from each magnetization pattern is different, as shown in Figure 9c,d, and the radial magnetization pattern has the advantage that the magnetic flux is more concentrated than in the parallel magnetization pattern. In this paper, characteristic analysis was performed on two patterns to determine the pattern of magnetization. Finally, we applied the radial magnetization pattern to improve performance and reduce torque ripple. Table 4 shows the magnet specifications of the conventional spoke model and the proposed flared model. As shown in Table 4, the total use of permanent magnets in the initial model and in the proposed model is the same. This means that there is no increase in material cost due to permanent magnets. Although, the proposed flared type rotor structure is composed of a number of

magnets compared to the basic IPM model so the assembly cost can increase in the manufacturing process. However, it can be improved by using the assembly automation technology.
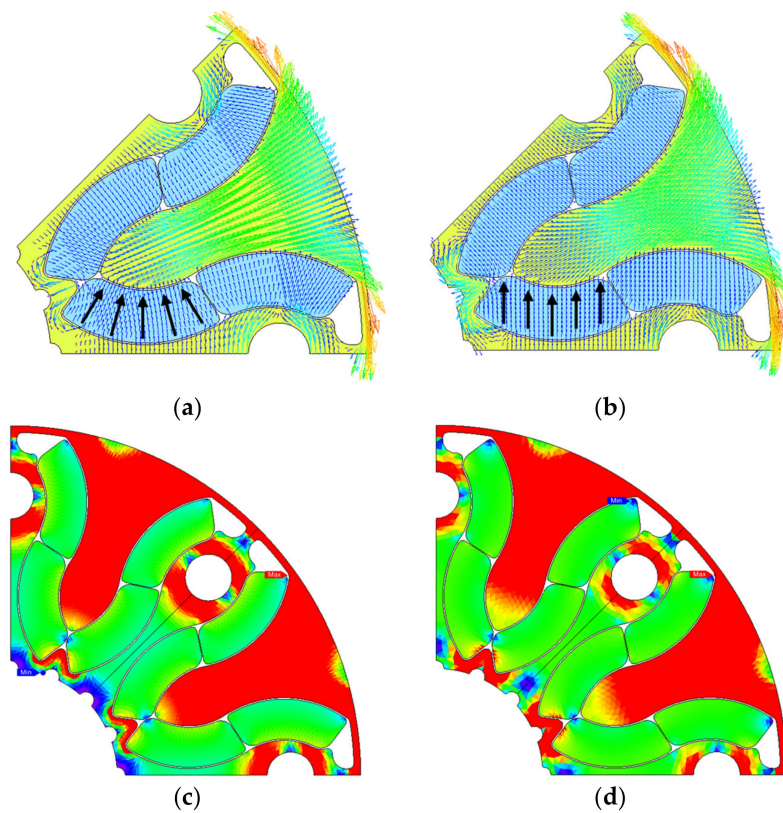

Figure 9. The magnetization direction of the proposed flared ferrite IPM model: (**a**) radial magnetization pattern; (**b**) parallel magnetization pattern; (**c**) flux density of radial magnetization pattern; (**d**) flux density of parallel magnetization pattern.

Table 4. Magnet specifications of the conventional spoke model and the proposed flared model.

Item	Unit	Basic Model	Proposed Model
Material	-	YBM-9BE (Ferrite)	YBM-9BE (Ferrite)
Magnet shape	-	Bar-type	C-type
Dimensions	mm	$16.5 \times 7.4t$	$70deg \times 3.4t$
Cross sectional area	mm^2	122.1	30.6
Height (z-axis)	mm	27.5	27.5
Total quantity	Ea	8	32
Total weight	g	134.3	134.3

3. Characteristics of Spoke Type IPM Model and Flared Type IPM Model

3.1. Characteristics at No-Load Condition

To examine the validity of the proposed model, the no-load analysis and the load analysis were performed, and the performance improvement was confirmed by comparing the results. Figure 10 shows the back EMF waveform at the no-load condition. Compared to the basic spoke type IPM model, the flared-shape structure of ferrite magnets has the advantage that magnetic flux is more concentrated in the central part of the rotor core as a result of the arrangement of C-shaped ferrite magnets. Therefore, the magnitude of back EMF of the proposed flared type IPM model in the no-load condition increased by 4.96% compared to that of the basic spoke type IPM model.
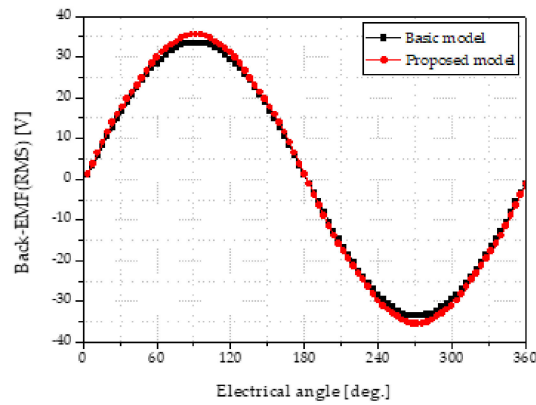
Figure 10. Characteristics of the back EMF waveform.

Figure 11 shows THD analysis of the back EMF waveforms. The THD of the back EMF is 1.47% which is higher than in the basic spoke type IPM model (0.69%). In general, the limit of THD is under 3.0% in the electrical vehicle and domestic appliance industries.
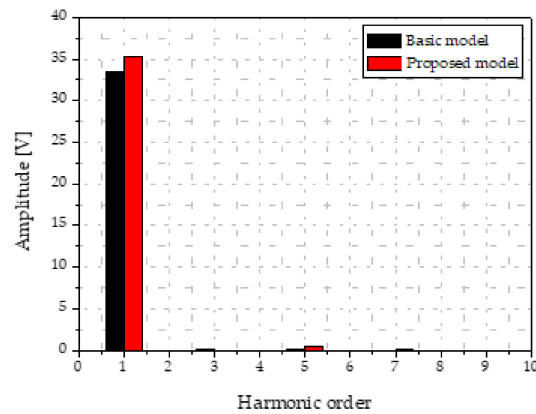

Figure 11. Characteristics of total harmonic distortion (THD) of the back EMF waveforms.

Figure 12 shows the cogging torque waveforms at no-load. The proposed flared type IPM model has increased effective magnetic flux due to the characteristic of magnetic flux concentration, and the cogging torque ripple is 17% higher compared to the basic spoke type IPM model. Although cogging torque ripple increased, the magnitude of the back EMF also increased; therefore, improved efficiency is expected because the current is reduced at the rated load.
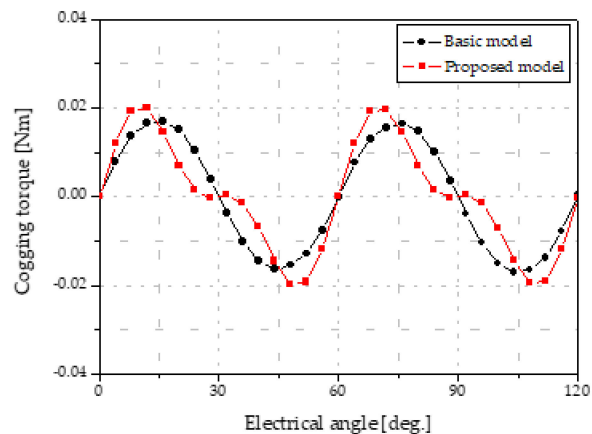

Figure 12. Characteristics of the cogging torque waveform.

Table 5 shows the 2D FEM analysis results of the proposed flared type IPM model in comparison with the basic spoke type IPM PMSM model.

Table 5. Comparison of the characteristics at no-load.

	Item	Unit	Basic Model	Proposed Model	Rate
No-Load (4020 rpm)	Back EMF	Vrms	23.65	24.82	▲4.96%
	THD	%	0.69	1.47	-
	Cogging torque ripple	Nm	0.034	0.040	▲16.97%

3.2. Characteristics at Load Condition

The surfaced permanent magnet motor is a structure in which permanent magnets are attached to the surface of the rotor. This structure has a constant magnetic resistance on the magnetic circuit, so there is no difference in inductance between the d and q axes. Therefore, it is difficult to generate additional reluctance torque, so the load analysis can be carried out by zero degrees of the advance angle for the current source analysis.

However, the IPM motor has different magnetic resistance on the d and q axes. This is because permanent magnets are inserted inside the rotor. The difference in magnetic resistance produces additional reluctance torque. Therefore, the basic model and the proposed model should set an advance angle by analyzing the changes in the torque according to the advance angle. Table 6 shows the average torque of the basic model and proposed model according to the advance angle. As a result of the torque analysis according to the advanced angle, both the basic model and the proposed model are found to have maximum torque at 5 degrees.

Table 6. Characteristics of torque according to the advance angle.

Item	Unit	−15	−10	−5	0	5	10	15
Basic model (at 6.00 Apeak)	Nm	0.680	0.698	0.711	0.719	0.722	0.718	0.710
Proposed model (at 5.47 Apeak)	Nm	0.667	0.688	0.704	0.714	0.719	0.718	0.711

Figure 13 shows the torque ripple of the proposed flared-shape IPM model compared to the basic spoke type IPM model. As shown in Figure 13, the average torque is equivalent and the torque ripple is reduced by 76.7% compared to the basic spoke type IPM model. So, the improvement of torque ripple at rated load has the advantage of reducing model noise and vibration. Therefore, the proposed flared type IPM model can be used in applications where noise and vibration improvements are required.
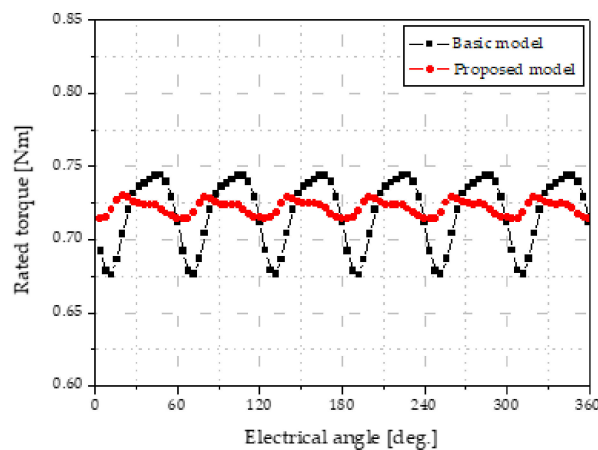

Figure 13. Torque waveform at rated load (at 4020 rpm).

Figure 14 shows the nodal force waveforms applied to stator teeth. When the nodal force by the electromagnetic force is applied to the stator teeth as an exciting force, it causes noise and vibration at operating point. In particular, the maximum change of the nodal force causes noise and vibration in the stator teeth. Therefore, the nodal force applied to stator teeth should be minimized during the initial design.
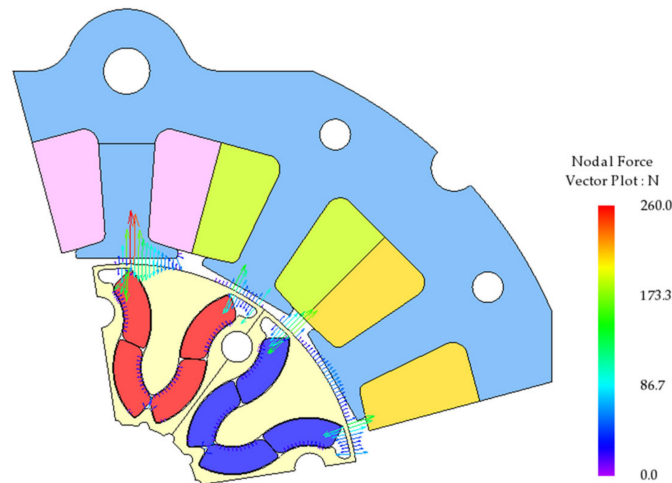

Figure 14. Nodal forces applied to stator teeth at the load condition.

Figure 15 shows the comparison of the nodal force of the proposed flared type IPM model compared to the basic spoke type IPM model at the operating point; as shown in Table 7, the average value of the nodal force of the proposed flared type IPM model is reduced by 3.0% compared to that of the basic spoke type IPM model.
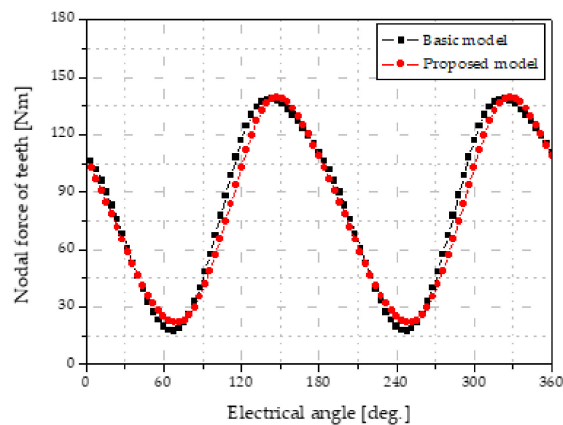

Figure 15. Comparison of the nodal force at the load condition.

Table 7. Comparison of nodal force of basic and proposed model.

Item		Unit	Basic Model	Proposed Model	Rate
Nodal force	x-axis	Nm	10.93	11.62	▲6.31%
(peak to peak)	y-axis	Nm	121.24	117.60	▼3.00%

Table 8 shows the 2D FEM analysis results of the proposed flared type IPM model in comparison with the basic spoke type IPM model. As shown in Table 8, the proposed flared-shape ferrite IPM model decreased copper loss by 16.3% and iron loss by 15.8%. The decrease in copper loss is due to the decrease in rated current caused by the back EMF increase. Additionally, iron loss was relatively reduced because the electrical steel usage of the rotors was reduced. Therefore, the efficiency of the

proposed flared type IPM model in the rated load condition is 1.2% higher than that of the basic spoke type IPM model. The torque ripple is also reduced by 76.6% compared to the basic spoke type IPM model. Table 9 shows the comparison of iron loss by part, and it can be confirmed that most of the iron loss reduction occurs in the rotors. Figure 16 shows a comparison of the flux density at the load condition.

Table 8. Comparison of finite element method (FEM) analysis results.

Item	Unit	Basic Model	Proposed Model	Rate
Rated speed	rpm	4020	4020	-
Torque (average)	Nm	0.72	0.72	-
Torque ripple	Nm	0.068 (9.4%)	0.016 (2.2%)	▼76.6%
Phase current	Apeak	6.00	5.49	▼8.5%
Current density	Arms/mm^2	9.43	8.63	▼8.5%
Output power	W	303.7	302.5	-
Copper loss	W	14.4	12.1	▼16.3%
Iron loss	W	9.3	7.8	▼15.8%
Efficiency	%	92.7	93.8	▲1.2%

Table 9. Comparison of iron loss by part.

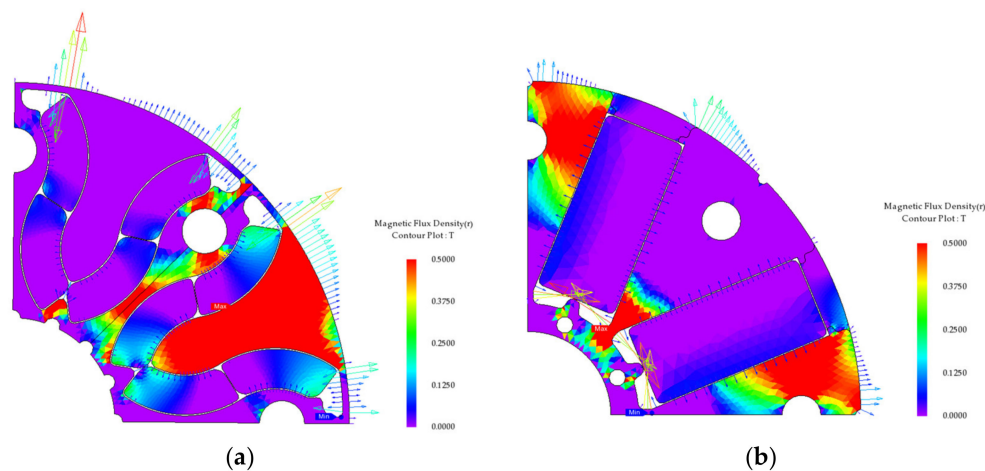| Item		Unit	Basic Model	Proposed Model	Rate
	Rotor	W	1.50	0.59	▼60.9%
Iron loss	Stator	W	6.46	5.97	▼7.6%
(Including Hysteresis)	Teeth	W	1.37	1.30	▼5.1%
	Total	W	9.33	7.86	▼15.8%

(a)   (b)

Figure 16. Comparison of the flux density at the load condition: (**a**) flux density of proposed flared type rotor; (**b**) flux density of basic spoke type rotor.

4. Experimental Verification

4.1. Prototype of Proposed model

To verify the performance improvement of the proposed flared IPM model, a real prototype was produced and studied. Figure 17 shows the prototype for the proposed flared IPM model. Figure 17a shows stator assembly, Figure 17b shows the rotor assembly, and Figure 17c shows the permanent magnet arrangement inside the rotor assembly. Stator winding was produced by the concentrated winding method. In order to prevent the deformation of the rotor during high-speed rotation, the rotor was manufactured using 8 bolting points. The magnet used 9BE grade ferrite and required 32 magnets.
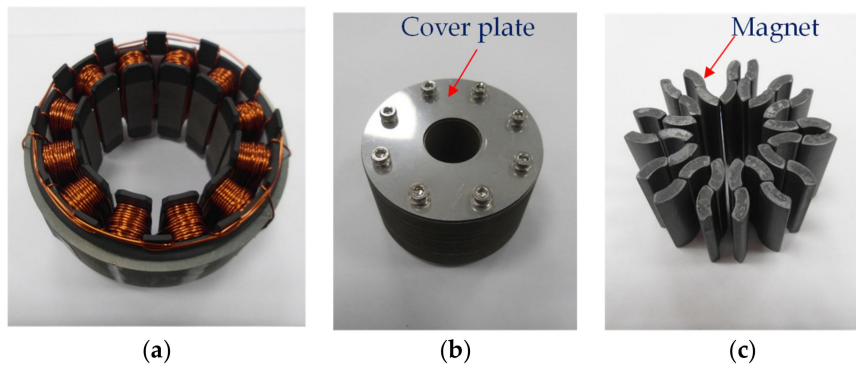
Figure 17. Prototype of the proposed model; (**a**) stator assembly; (**b**) rotor assembly; (**c**) magnet arrangement for flared shape.

4.2. Experimental Results

The load test was performed using the prototype. Figure 18 shows the torque waveform at rated load, and Table 10 shows a comparison of the basic spoke type model and the prototype of the proposed flared IPM model. As shown in Figure 18, the experimental results of the proposed flared IPM model were similar compared to the analytical values. Additionally, torque ripple decreased by 66.2%, and efficiency improved by 0.9%. This confirms the performance improvement of the proposed model.
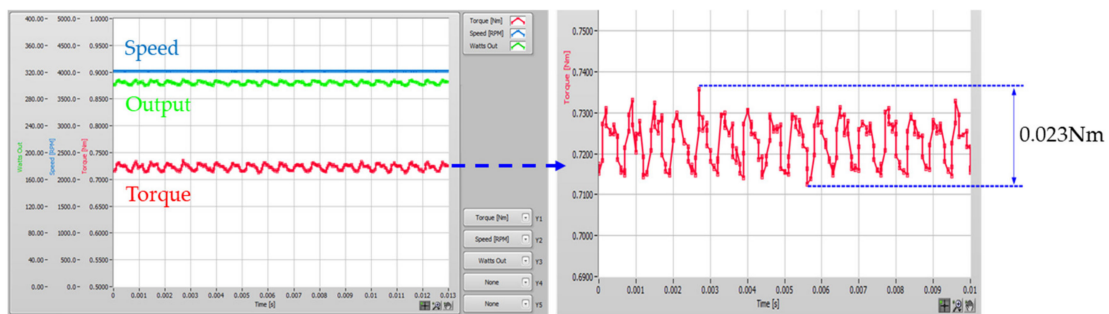

Figure 18. Experimental characteristics at rated load test (at 4020 rpm) and enlarged torque ripple waveform.

Table 10. Comparison of the basic model and the prototype model.

| Item | Unit | Basic Model | Proposed Model | | Rate |
		Analysis	Analysis	Experiment	
Average torque	Nm	0.72	0.72	0.72	-
Torque ripple	Nm	0.068 (9.4%)	0.016 (2.2%)	0.023 (3.2%)	▼66.2%
Output power	W	303.7	302.5	304.1	-
Efficiency	%	92.7	93.8	93.6	▲0.9%

5. Conclusions

In this paper, we proposed the flared type ferrite IPM model as an alternative to the basic spoke type ferrite IPM model. As a result of the experimental results of the proposed flared IPM model, the efficiency was increase by 0.9% and torque ripple was reduced by 66.2% compared to the basic spoke type ferrite IPM PMSM motor. Therefore, the comparison using the results of FEM analysis and the prototype experiment showed that the proposed flared IPM model is an effective substitute for the basic spoke type IPM model requiring the same output. In particular, the proposed flared type IPM model has lower torque ripple and higher efficiency than the basic spoke type IPM model. The proposed flared type IPM model also has a low nodal force ripple, giving it an advantage for acoustic noise and vibration. Through the analysis and experimental verification, we can confirm

that the proposed flared type IPM model is an excellent alternative possibility for applications that require low cost, high output, and low noise and vibration. Forward, we will conduct a noise vibration experiment for the prototype to verify the improvement effect and optimize the proposed flared type IPM model.

Author Contributions: Conceptualization, K.-Y.Y.; methodology, K.-Y.Y.; software, K.-Y.Y.; validation, K.-Y.Y. and S.-W.B.; writing—original draft preparation, K.-Y.Y.; writing—review and editing, K.-Y.Y.; and S.-W.B. funding acquisition, S.-W.B. All authors have read and agreed to the published version of the manuscript.

Conflicts of Interest: The authors declare no conflict of interest.

References

1. El-Refaie, A.; Jahns, T.; McCleer, P.; McKeever, J. Experimental verification of optimal flux weakening in surface PM Machines using concentrated windings. *IEEE Trans. Ind. Appl.* **2006**, *42*, 443–453. [CrossRef]
2. Dutta, R.; Rahman, F. Design and Analysis of an Interior Permanent Magnet (IPM) Machine With Very Wide Constant Power Operation Range. *IEEE Trans. Energy Convers.* **2008**, *23*, 25–33. [CrossRef]
3. Kim, S.-I.; Cho, J.; Park, S.; Park, T.; Lim, S. Characteristics Comparison of a Conventional and Modified Spoke-Type Ferrite Magnet Motor for Traction Drives of Low-Speed Electric Vehicles. *IEEE Trans. Ind. Appl.* **2013**, *49*, 2516–2523. [CrossRef]
4. Kim, S.; Park, S.; Park, T.; Cho, J.; Kim, W.; Lim, S. Investigation and Experimental Verification of a Novel Spoke-Type Ferrite-Magnet Model for Electric-Vehicle Traction Drive Applications. *IEEE Trans. Ind. Electron.* **2014**, *61*, 5763–5770.
5. Kim, H.-J.; Kim, D.-Y.; Hong, J.-P. Structure of Concentrated-Flux-Type Interior Permanent-Magnet Synchronous Motors Using Ferrite Permanent Magnets. *IEEE Trans. Magn.* **2014**, *50*, 1–4. [CrossRef]
6. Ohnishi, T.; Takahashi, N. Optimal Design of Efficient IPM Model Using Finite Element Method. *IEEE Trans. Magn.* **2000**, *36*, 3537–3539. [CrossRef]
7. Rahman, M.M.; Kim, K.-T.; Hur, J. Design and Optimization of Neodymium-Free SPOKE-Type Motor With Segmented Wing-Shaped PM. *IEEE Trans. Magn.* **2014**, *50*, 865–868. [CrossRef]
8. Parasiliti, F.; Villaini, M.; Lucidi, S.; Rinaldi, F. Finite-Element-Based Multiobjective Design Optimization Procedure of Interior Permanent Magnet Synchronous Model for Wide Constant-Power Region Operation. *IEEE Trans. Ind. Electron.* **2012**, *59*, 2503–2514. [CrossRef]
9. Fang, L.; Jung, J.-W.; Hong, J.-P.; Lee, J.-H. Study on High-Efficiency Performance in Interior Permanent-Magnet Synchronous Motor With Double-Layer PM Design. *IEEE Trans. Magn.* **2008**, *44*, 4393–4396. [CrossRef]
10. Lee, J.-H.; Kwon, B.-I. Optimal Rotor Shape Design of a Concentrated Flux IPM-Type Motor for Improving Efficiency and Operation Range. *IEEE Trans. Magn.* **2013**, *49*, 2205–2208. [CrossRef]
11. Kim, J.-M.; Chai, S.-H.; Yoon, M.-H.; Hong, J.-P. Plastic Injection Molded Rotor of Concentrated Flux-Type Ferrite Magnet Motor for Dual-Clutch Transmission. *IEEE Trans. Magn.* **2015**, *51*, 1–4. [CrossRef]
12. Kim, K.-S.; Park, M.-R.; Kim, H.-J.; Chai, S.-H.; Hong, J.-P. Estimation of Rotor Type Using Ferrite Magnet Considering the Magnetization Process. *IEEE Trans. Magn.* **2015**, *52*, 1–4. [CrossRef]
13. Park, M.-R.; Jung, J.-W.; Kim, D.-Y.; Hong, J.-P.; Lim, M.-S. Design of High Torque Density Multi-Core Concentrated Flux-Type Synchronous Motors Considering Vibration Characteristics. *IEEE Trans. Ind. Appl.* **2018**, *55*, 1351–1359. [CrossRef]
14. Park, J.-H.; Jung, K.-T.; Jung, Y.-H.; Lim, M.-S.; Yoon, M.-H.; Hong, J.-P.; Jung, J.-W. Design and Verification for the Torque Improvement of a Concentrated Flux-Type Synchronous Motor for Automotive Applications. *IEEE Trans. Ind. Appl.* **2019**, *55*, 3534–3543. [CrossRef]
15. Wang, Q.; Zhao, B.; Zhao, H.; Li, Y.; Zou, J. Optimal Design of Tubular Transverse Flux Motors With Low Cogging Forces for Direct Drive Applications. *IEEE Trans. Appl. Supercond.* **2016**, *26*, 1–5. [CrossRef]
16. Bianchini, C.; Immovilli, F.; Lorenzani, E.; Bellini, A.; Davoli, M. Review of Design Solutions for Internal Permanent-Magnet Machines Cogging Torque Reduction. *IEEE Trans. Magn.* **2012**, *48*, 2685–2693. [CrossRef]

17. Bianchini, C.; Davoli, M.; Immovilli, F.; Lorenzani, E. Design optimization for torque ripple minimization and poles cost reduction with hybrid permanent magnets. In Proceedings of the IECON 2014 - 40th Annual Conference of the IEEE Industrial Electronics Society, Dallas, TX, USA, 29 October–1 November 2014; Institute of Electrical and Electronics Engineers (IEEE): Piscataway, NJ, USA; Volume 40, pp. 483–489.

18. Yang, X.; Kou, B.; Luo, J.; Zhou, Y.; Xing, F. Torque Characteristic Analysis of a Transverse Flux Motor Using a Combined-Type Stator Core. *Appl. Sci.* **2016**, *6*, 342. [CrossRef]

19. Kappatou, J.; Zalokostas, G.D.; Spyratos, D.A. 3-D FEM Analysis, Prototyping and Tests of an Axial Flux Permanent-Magnet Wind Generator. *Energies* **2017**, *10*, 1269. [CrossRef]

20. Zou, J.; Zhao, M.; Wang, Q.; Zou, J.; Wu, G. Development and Analysis of Tubular Transverse Flux Machine With Permanent-Magnet Excitation. *IEEE Trans. Ind. Electron.* **2011**, *59*, 2198–2207. [CrossRef]

21. Doering, J.; Steinborn, G.; Hofmann, W.; Doring, J. Torque, Power, Losses, and Heat Calculation of a Transverse Flux Reluctance Machine With Soft Magnetic Composite Materials and Disk-Shaped Rotor. *IEEE Trans. Ind. Appl.* **2014**, *51*, 1494–1504. [CrossRef]

22. Yoon, K.-Y.; Lee, J.-H.; Kwon, B.-I. Characteristics of new interior permanent magnet motor using flared-shape arrangement of ferrite magnets. *Int. J. Appl. Electromagn. Mech.* **2016**, *52*, 591–597. [CrossRef]

23. Yoon, K.-Y.; Kwon, B.-I. Optimal Design of a New Interior Permanent Magnet Motor Using a Flared-Shape Arrangement of Ferrite Magnets. *IEEE Trans. Magn.* **2016**, *52*, 1–4. [CrossRef]

24. Lin, C.; Fahimi, B. Prediction of Radial Vibration in Switched Reluctance Machines. *IEEE Trans. Energy Convers.* **2013**, *28*, 1072–1081. [CrossRef]

25. Callegaro, A.D.; Liang, J.; Jiang, J.W.; Bilgin, B.; Emadi, A. Radial Force Density Analysis of Switched Reluctance Machines: The Source of Acoustic Noise. *IEEE Trans. Transp. Electrif.* **2018**, *5*, 93–106. [CrossRef]